

Giant Hall effect in two-dimensional CoSi₂ granular arraysElica Anne Heredia,¹ Shao-Pin Chiu², Ba-Anh-Vu Nguyen,³ Ruey-Tay Wang,³ Chih-Yuan Wu,² Sheng-Shiuan Yeh^{1,4,*} and Juhn-Jong Lin^{3,†}¹*International College of Semiconductor Technology, National Yang Ming Chiao Tung University, Hsinchu 30010, Taiwan*²*Department of Physics, Fu Jen Catholic University, Taipei 24205, Taiwan*³*Department of Electrophysics, National Yang Ming Chiao Tung University, Hsinchu 30010, Taiwan*⁴*Center for Emergent Functional Matter Science, National Yang Ming Chiao Tung University, Hsinchu 30010, Taiwan*

(Received 22 March 2024; revised 10 June 2024; accepted 24 June 2024; published 8 July 2024)

Granular metals offer tailorable electronic properties and play crucial roles in device and sensor applications. We have fabricated a series of nonmagnetic granular CoSi₂ thin films and studied the Hall effect and transport properties. We observed a two-order magnitude enhancement in the Hall coefficient in films that fall slightly above the metal-insulator transition. This giant Hall effect (GHE) is ascribed to the local quantum-interference effect-induced reduction of the charge carriers. Transmission electron microscopy images and transport properties indicate that our films form quasi-two-dimensional granular arrays. The GHE may provide useful and sensitive applications.

DOI: [10.1103/PhysRevB.110.024201](https://doi.org/10.1103/PhysRevB.110.024201)**I. INTRODUCTION**

Granular metals, M_xI_{1-x} , are composites comprising metals (M) and insulators (I), where x denotes the volume or area fraction of M [1]. In granular composites, the size of metallic particles typically ranges from a few to hundreds of nanometers. Granular metals are inhomogeneously disordered, and form either three-dimensional (3D) or two-dimensional (2D) arrays, depending on the metal grain size relative to film thickness. They can be considered as artificial solids with engineerable electronic and optical characteristics [2]. They serve as not only useful materials for nanotechnology applications but also controllable systems for exploring the quantum-interference and electron-electron interaction (EEI) effects [2,3] as well as the percolation problem [1]. In practice, research on granular composites has led to the development of chemical sensors [4,5], strain gauges [6,7], temperature-insensitive resistors [8], etc.

The Hall coefficient R_H provides important information about the charge carrier density (n^*) and polarity of a conductor. The knowledge of R_H of granular metals, especially its behavior near the percolation threshold or the metal-insulator transition (MIT), is of particular interest. According to the classical percolation theory, R_H is sensitive to the dimensionality of the system [9–12]. In 3D, the theory predicts that as x decreases from 1, R_H monotonically increases and takes a maximum value at the classical percolation threshold (x_c). In 2D, the theory predicts that R_H retains the same value as that of the pure metal in the entire metallic regime ($x \geq x_c$). These classical predictions for the 3D case [13] and 2D case [14] were previously observed in experiments. In this work,

we report an enhancement of R_H by a factor ≈ 100 as x approaches the quantum percolation threshold, denoted by x_q ($> x_c$), in a series of nonmagnetic CoSi₂ thin films which form quasi-2D granular arrays. To our knowledge, such giant Hall effect (GHE) in 2D nonmagnetic granular arrays has never been previously found. We interpret that the GHE arises from a reduction of n^* due to the carrier localization induced by the local quantum interference effect in an inhomogeneously disordered system containing rich microstructures [15]. We mention that a continuous CoSi₂ film is a good metal with its temperature (T) behavior of resistivity well described by the Boltzmann transport equation; until it undergoes superconducting transition at about 1.5 K [16].

II. EXPERIMENTAL METHOD

A series of CoSi₂ thin films with various thicknesses, and thus grain sizes, were grown on ≈ 300 -nm-thick SiO₂ capped Si substrates. A Si layer with thickness t_{Si} was deposited on the substrate via thermal evaporation in a high vacuum ($\sim 2 \times 10^{-6}$ torr), followed by the evaporation deposition of a Co layer of thickness t_{Co} . The ratio $t_{\text{Si}} = 3.6 t_{\text{Co}}$ was chosen to ensure a complete reaction between Co and Si to form the CoSi₂ phase in the subsequent thermal annealing process [17]. After the thermal annealing process, the thickness t of the resulted CoSi₂ film was expected to be $t \simeq 3.5 t_{\text{Co}}$, as previously established [18]. This series of films, called group A, had thickness t in the range $11 < t < 52$ nm and formed a 2D granular array. A second series of CoSi₂ films, called group B, with $33 < t < 105$ nm was grown via the deposition of a t_{Co} thick Co layer directly on a high-purity Si(100) substrate. The as-deposited groups A and B films were annealed in a high vacuum ($\sim 1 \times 10^{-6}$ torr) at 600–800°C for 1 h to form the CoSi₂ phase. The CoSi₂ structure was polycrystalline in group A, while nominally epitaxial in group B [17]. To

*Contact author: ssyeh@nycu.edu.tw†Contact author: jjlin@nycu.edu.tw

TABLE I. Relevant parameters of CoSi₂ films. t is film thickness, a_{AFM} is mean diameter of CoSi₂ grains, k_F is Fermi wave number, ℓ_e is elastic mean free path at 2 K, and L_φ is dephasing length.

Film	t (nm)	a_{AFM} (nm)	$k_F \ell_e$	L_φ (2 K) (nm)
A11	11	12	1.0	40
A14	14	20	1.5	38
A18	18	26	3.1	47
A20	20	28	5.1	40
A20.5	20.5	30	8.3	–
A21	21	32	10	57
A22	22	32	10	–
A23	23	35	11	69
A35	35	47	21	100
A52	52	51	24	130
B33	33	52	310	690
B70	70	60	510	1300
B105	105	330	540	1400

facilitate transport measurements, a metal shadow mask was used during the deposition process to define a Hall bar geometry of 1 mm wide and 1 mm long. The relevant parameters of our films are listed in Table I.

The topography of the CoSi₂ film surface was characterized by atomic force microscopy (AFM) (DFM SPA 400). The cross-sectional transmission electron microscopy (TEM) studies were performed using a high-resolution transmission electron microscope (JEOL JEM-F200). Four-probe electrical and Hall effect measurements were carried out using a closed-cycle refrigerator and a ³He fridge.

III. RESULTS AND DISCUSSION

A. Giant Hall effect in quasi-2D CoSi₂ granular arrays

In Fig. 1(a), the surface topography for three group A and one group B CoSi₂ films measured by AFM reveals mountain peaklike profiles. Assuming these peaks reflect the profiles of the surfaces of the constituent grains and grains are spherical, we estimate the average grain size (a_{AFM}) in each film using the Gwyddion software (version 2.61). The data gathered from the AFM images were first leveled by mean plane subtraction,

followed by row aligning using the median and matching methods. Horizontal scars or strokes were corrected to ensure accuracy, followed by color mapping to aid in selecting the appropriate range for analysis. Individual grains were then identified by selecting a threshold height of 50 percent, and all grain sizes within a 1- μm^2 area were measured and averaged. The obtained a_{AFM} values are listed in Table I.

Figure 1(b) shows the variation of a_{AFM} with t . For the B105 film, we obtain $a_{\text{AFM}} \approx 330$ nm, which is close to that determined from the scanning electron microscopy (SEM) and the TEM images [19]. For group A films, as t increases from 11 to 52 nm, a_{AFM} increases from ≈ 12 to ≈ 50 nm. For group B films, as t increases from 33 to 105 nm, a_{AFM} increases from ≈ 50 to ≈ 330 nm. We note that, in every film, $a_{\text{AFM}} \gtrsim t$. The distribution of the grain size can be approximately described by a Gaussian form, with a standard deviation of $\approx 58\%$ of the average grain size a_{AFM} in each film. Also in each film, the ratio of the number of grains with sizes smaller than t to the total number of grains can be analyzed; and was found to be $\approx 33\%$. These results imply that all of our films are essentially constituted of a single layer of CoSi₂ grains. The TEM images in Fig. 1(c) and those from our previous work [19] also confirm this assertion. Thus, our CoSi₂ films form quasi-2D granular arrays. Moreover, considering that the GHE arises from a quantum-interference effect [20] and that we have the electron dephasing length $L_\varphi(2\text{ K}) > t$ in every film (Table I), our observed GHE can then be safely ascribed to a 2D phenomenon (see further discussion below), where L_φ is the characteristic length scale governing the system dimensionality of the quantum-interference transport behaviors.

We have measured the longitudinal resistivity ρ_{xx} and R_H of our films and obtained n^* from $n^* = 1/eR_H$. The Hall effect measurements indicate that the charge carriers are holes, in consistency with our previous results [16,17] and band structure calculations [21,22]. The elastic electron mean free path ℓ_e is then calculated through $\rho_{xx}^{-1} = k_F^2 e^2 \ell_e / (3\pi^2 \hbar)$, with the Fermi wave number $k_F = (3\pi^2 n^*)^{1/3}$. The value of the product $k_F \ell_e$ for every film is listed in Table I. Figure 2 shows the normalized resistivity, $\rho_{xx}(T)/\rho_{xx}(2\text{ K})$, as a function of T for several group A films between 2 and 10 K. We see that those films having $t \gtrsim 20$ nm exhibit metallic behavior, i.e., ρ_{xx} increases

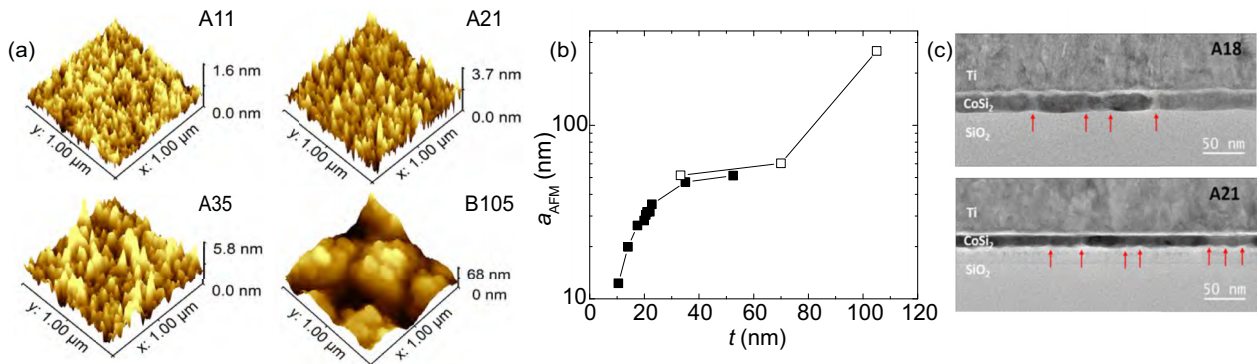


FIG. 1. (a) AFM images for four films, as indicated. (b) Average grain size a_{AFM} as a function of film thickness t . Solid (open) symbols denote group A (B) films. (c) Cross-sectional TEM images for films A18 and A21. Red arrows indicate the boundaries between neighboring CoSi₂ grains.

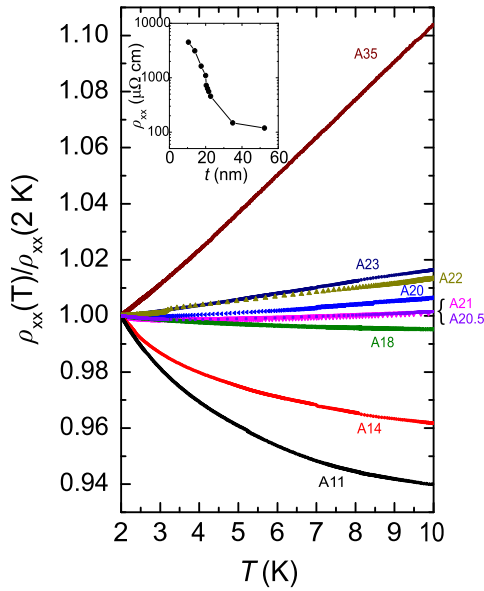


FIG. 2. Normalized longitudinal resistivity $\rho_{xx}(T)/\rho_{xx}(2\text{ K})$ as a function of T for group A films, as indicated. Inset: Variation of $\rho_{xx}(2\text{ K})$ with t for group A films.

with increasing T ; while those films having $t \lesssim 18\text{ nm}$ reveal insulating behavior, i.e., ρ_{xx} decreases with increasing T . Thus, the metal-insulator transition occurs around $t \simeq 19\text{ nm}$. In other words, for films with $t \gtrsim 20\text{ nm}$, the neighboring CoSi₂ grains are geometrically connected, forming a percolating conduction array. For films with $t \lesssim 18\text{ nm}$, the CoSi₂ grains are geometrically disconnected. The inset of Fig. 2 shows $\rho_{xx}(2\text{ K})$ as a function of t . As t decreases from 53 to 11 nm, $\rho_{xx}(2\text{ K})$ increases rapidly from 131 to 4230 $\mu\Omega\text{ cm}$, indicating that the granularity plays an increasingly important role especially when t decreases to below about 20 nm. For comparison, $\rho_{xx}(2\text{ K}) = 4.55, 2.70,$ and $2.50\ \mu\Omega\text{ cm}$ for nominally continuous films B33, B70, and B105, respectively.

Figure 3 shows R_H as a function of ρ_{xx} at $T = 2\text{ K}$. The thickest film B105 has the lowest Hall coefficient $R_H \simeq 2.5 \times 10^{-10}\text{ m}^3/\text{C}$, in agreement with the previous result

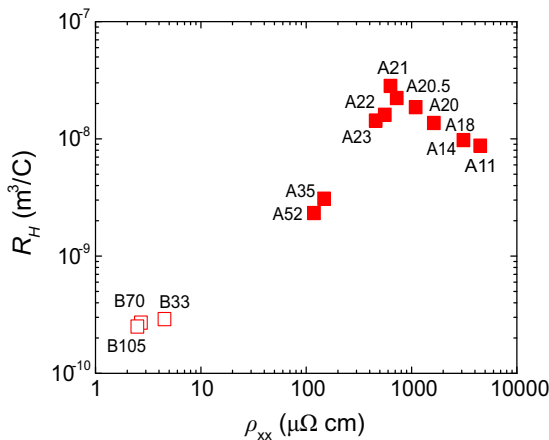


FIG. 3. Hall coefficient R_H as a function of ρ_{xx} for granular group A and nominally epitaxial group B films at $T = 2\text{ K}$.

[23,24]. This film will serve as our reference film with the R_H value for a good CoSi₂ metal. Note that for films A21–A52, R_H monotonically increases with increasing ρ_{xx} , reaching a maximum value of $\approx 2.8 \times 10^{-8}\text{ m}^3/\text{C}$ (corresponding to $n^* \approx 2.2 \times 10^{26}\text{ m}^{-3}$) in film A21. This is a film falling just above the MIT. Interestingly, as ρ_{xx} further increases (i.e., t further decreases), R_H progressively decreases to $\approx 8.7 \times 10^{-9}\text{ m}^3/\text{C}$ in film A11, which falls below the MIT. We emphasize that the R_H value of film A21 is ≈ 100 times larger than that of film B105. This is the GHE [20]. Recall that according to the classical percolation theory [15,25], $R_H(x \rightarrow x_c)$ will be enhanced by a factor $\sim (t/a)^{\tilde{g}/\nu}$, where \tilde{g} is the critical exponent of Hall resistivity, ν is the exponent of the correlation length, and a is the grain size. However, for a 2D percolation system, $\tilde{g} = 0$ (Ref. [11]) and $\nu = 4/3$ (Ref. [26]), thus R_H should remain constant in the entire metallic regime ($x \geq x_c$), as mentioned [9–12]. This prediction was confirmed by a previous study of 2D granular Au films [14]. On the other hand, $\tilde{g} = 0.4$ and $\nu = 0.9$ in 3D, thus an enhancement of $R_H(x_c)$ by a factor of ~ 10 is expected for, e.g., a thick granular film with $t = 1\ \mu\text{m}$ and $a = 10\text{ nm}$. The GHE means that the measured $R_H(x \rightarrow x_q)$ value is orders of magnitude larger than the classical $R_H(x \rightarrow x_c)$ value.

In 1996, Pakhomov *et al.* found a GHE in ferromagnetic metal-insulator Ni₈₅Fe₁₅ – SiO₂ granular films [27], where they explained it in terms of the spin-dependent scattering off magnetic disorder. Subsequently, observations of the GHE in various magnetic metal-insulator composites were reported by several groups [28–31]. On the other hand, in 2001 Zhang *et al.* [15] found a GHE in 3D nonmagnetic Cu_{*x*}(SiO₂)_{1–*x*} granular metal films. To explain the latter observation in the absence of magnetic disorder, Wan and Sheng [20] have developed a quantum percolation theory that considers the wave nature of the charge carriers in a 3D nonmagnetic granular system. At low T , when the electron dephasing length L_φ is larger than the feature size (ξ) of the microstructures, the carrier wave functions will undergo multiple scattering in the random percolating clusters of the conducting channels until a phase-breaking event takes place. Such multiple coherent scattering leads to a local quantum-interference effect which causes significant localization of carrier wave functions as $x \rightarrow x_q$. Consequently, n^* will be greatly reduced, which in turn gives rise to a greatly enhanced R_H at $x \simeq x_q (> x_c)$. This theory has successfully explained the GHE observed in 3D nonmagnetic Cu_{*x*}(SiO₂)_{1–*x*} composites [15] and Mo_{*x*}(SnO₂)_{1–*x*} composites [25], where an enhancement by a factor of nearly three orders of magnitude in $R_H(x \rightarrow x_q)$ was observed. Due to this local quantum interference effect, which is absent in the classical percolation theory, R_H peaks at a metal volume fraction $x_q > x_c$. The GHE in 2D has not been theoretically treated in the literature.

To clarify the underlying physics for the GHE observed in the group A films, we have measured the weak-localization induced magnetoresistance [32] at low T and extracted L_φ for each film, see Table I. The $L_\varphi(2\text{ K})$ values in group B nominally epitaxial films are much longer than those in group A polycrystalline films, as expected. In both cases, L_φ decreases with decreasing t , due to an increasing dephasing rate as the disorder is increased with decreasing t and decreasing a_{AFM} . Most importantly, we obtain $L_\varphi(2\text{ K}) > \xi \sim a_{\text{AFM}} >$

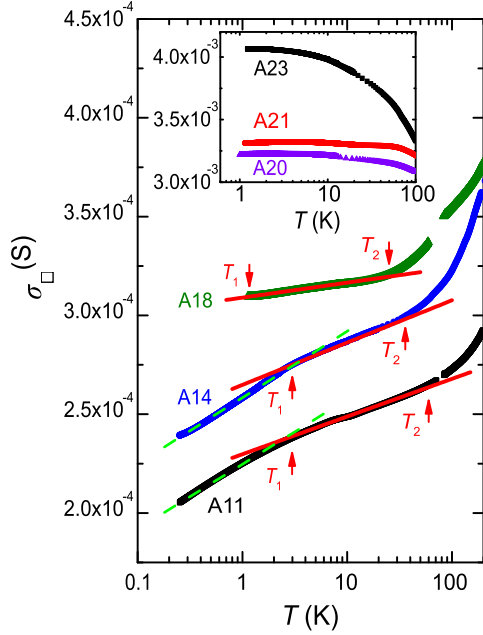


FIG. 4. Sheet conductivity σ_{\square} as a function of T for films A11, A14, and A18. The data of A14 (A18) are offset by -2×10^{-4} (-7.6×10^{-4}) S, for clarity. Inset: σ_{\square} as a function of T for films A20, A21 and A23. The data of A20 (A23) are offset by 1.4×10^{-3} (-9×10^{-4}) S, for clarity.

t in all films, indicating that our granular arrays are 2D concerning the quantum-interference transport phenomena. Consequently, multiple coherent electron scattering within a characteristic area of L_{φ}^2 leads to a quasi-2D local quantum interference effect, resulting in a reduced n^* and an enhanced R_H [15,20].

In the percolation theory, the relevant parameter is the metal volume (area) fraction x , which cannot be accurately determined in our films. Nevertheless, we know that x_c occurs around $t \approx 19$ nm where the MIT takes place. On the other hand, we may assume x_q occurs around $t \approx 21$ nm where the R_H value peaks. This is in consistency with the above quantum percolation theory prediction that $x_q > x_c$ [20]. At this critical thickness, one expects the film to have a value of the product $k_F \ell_e \sim 2\pi$, i.e., the Ioffe-Regel criterion, see Table I. Thus, our observation of the 2D version of the GHE is satisfactorily understood.

B. Transport in quasi-2D CoSi₂ granular arrays

To further clarify the occurrence of the GHE and the array dimensionality (\tilde{d}) of group A films, we study their longitudinal transport behavior. Figure 4 shows the sheet conductivity σ_{\square} as a function of T for films A11, A14, and A18, which have $x < x_c$. We find a $\sigma_{\square} \propto \ln T$ dependence in the temperature regime $T_1 < T < T_2$, with $T_1 \approx 3, 3,$ and 1.2 K, and $T_2 \approx 60, 37,$ and 16 K, for films A11, A14, and A18, respectively. This $\ln T$ behavior does not originate from the 2D EEI effect of Altshuler and Aronov (AA) [33], which considers homogeneously disordered metal films. To rule out this scenario, we may first assume our films to be homogeneously disordered and calculate the thermal

TABLE II. Relevant parameters for three films. E_c is the charging energy, a is the grain diameter calculated from E_c , g_T is the dimensionless intergranular tunneling conductance, and T^* is a crossover temperature defined in the text.

Film	E_c/k_B (K)	a (nm)	g_T	T^* (K)
A11	600	11	2.8	6.6
A14	370	18	4.4	2.5
A18	160	42	27	1.3

diffusion length $L_T = \sqrt{D\hbar/k_B T}$, where $D = \hbar k_F \ell_e / 3m^*$ is the diffusion constant, \hbar is the reduced Planck constant, and m^* is the effective electron mass. (We take m^* to be the free electron mass [23]). We obtain $L_T < t$ in the regime $T_1 < T < T_2$ for films A11, A14, and A18. This implies that these films, if homogeneously disordered, should be 3D concerning the AA EEI effect, then the conductivity correction must obey a \sqrt{T} temperature dependence [33]. This is not the case.

In fact, our results must be explained by the electron tunneling conduction in the presence of the EEI effect in a granular array. In the strong intergranular coupling regime with $g_T > g_c$, the transport properties of granular metals have been theoretically addressed [2], where g_T is a dimensionless tunneling conductance between neighboring grains, $g_c = (1/2\pi\tilde{d}) \ln(E_c/\tilde{\delta})$ is a critical conductivity, $E_c = e^2/4\pi\epsilon_0\epsilon_r a$ is the charging energy with ϵ_0 (ϵ_r) being the permittivity of vacuum (dielectric constant of I), and $\tilde{\delta}$ is the mean energy level spacing in a grain. The granular metal theory predicts that in the temperature regime $T^* = g_T \tilde{\delta} / k_B \leq T \ll E_c$ (k_B is the Boltzmann constant), incoherent tunneling processes on scales approximately equal to the grain size a play a pivotal role in governing the system conductivity, causing a conductivity correction ($\delta\sigma_1$). As the temperature further decreases to $T < T^*$, the coherent electron motion on scales larger than a becomes important, causing another conductivity correction ($\delta\sigma_2$). Thus, the total conductivity is given by $\sigma(T) = \sigma_0 + \delta\sigma_1(T) + \delta\sigma_2(T)$, where $\sigma_0 = (2e^2/\hbar)g_T a^{2-\tilde{d}}$ is the conductivity without the EEI effect,

$$\delta\sigma_1(T) = -\frac{\sigma_0}{2\pi g_T \tilde{d}} \ln \left[\frac{g_T E_c}{\max(k_B T, g_T \tilde{\delta})} \right], \quad (1)$$

and, for $\tilde{d} = 2$,

$$\delta\sigma_2(T) = -\frac{\sigma_0}{4\pi^2 g_T} \ln \left(\frac{g_T \tilde{\delta}}{k_B T} \right). \quad (2)$$

We note that the $\delta\sigma_2$ term reproduces the AA EEI effect by taking the screening factor \tilde{F} to be zero.

Figure 4 shows that our results can be well described by the predictions (red straight lines) of Eq. (1) in the intermediate T regime. For a quantitative analysis, we may take $E_c \approx 10k_B T_2$ (Ref. [34]) and $\epsilon_r \approx 2.5$ to estimate a [35]. The a value thus obtained (see Table II) is comparable with the corresponding a_{AFM} value. From the fitted σ_0 and g_T values, the T^* values can be calculated with $\tilde{\delta} \approx 1/\nu_0 a^3$, where ν_0 is the density of

states (DOS) at the Fermi energy of the free-electron model. The g_c values can also be calculated. We obtain $T^* \approx T_1$ and $g_T > g_c$ for each film, supporting the interpretation in terms of the $\delta\sigma_1$ correction. Moreover, below T^* , a crossover to the $\delta\sigma_2$ correction is observed in the two most granular films, A11 and A14, as indicated by the fitted green dashed straight lines given by Eq. (2) [36]. Thus, the results of Fig. 4 over the wide temperature from 0.25 K to T_2 indicate that our films form quasi-2D, rather than 3D, granular arrays. This conclusion is in line with the 2D granular array structure determined from the AFM and TEM images discussed above.

The inset of Fig. 4 shows that films A20, 21, and 23 reveal metallic behavior, with σ_{\square} increasing with decreasing T . This result further supports the GHE theory prediction that R_H should peak at $x_q > x_c$. Furthermore, we note that the large R_H enhancement in film A21 cannot be ascribed to the suppression of DOS. The granular metal theory has calculated the corrections to the DOS due to the EEI effect in the presence of granularity [37,38]. For $\tilde{d} = 2$ and at $T \lesssim T^*$, the correction to the DOS at the Fermi energy ($\delta\nu_2$) is given by $\delta\nu_2/\nu_0 = -(16\pi^2 g_T)^{-1} [\ln(g_T \delta/k_B T) \ln(g_T E_c^4/k_B T \delta^3 + 2 \ln^2(E_c/\delta))]$. This result indicates that a smaller grain size (a larger E_c) and a smaller g_T will cause a larger $|\delta\nu_2|$. Consider, for example, film A18. From the values $E_c/k_B \sim 160$ K and $g_T \sim 27$, we estimate $\delta\nu_2/\nu_0 \approx -3\%$, which would lead to a $\sim 3\%$ increase in R_H through the relation $\delta n^*/n^* \propto \delta\nu_2/\nu_0$, where δn^* is a correction to n^* . For the more continuous and less granular film A21, $\delta\nu_2/\nu_0$ should be smaller than that in film

A18. This small correction of DOS certainly cannot explain the observed GHE.

IV. CONCLUSION

We have fabricated a series of two-dimensional granular CoSi₂ films which encompasses the metal-insulator transition. We observe an enhanced Hall coefficient by a factor of ≈ 100 , which occurs in a film falling slightly above the metal-insulator transition. We explain this result in terms of the giant Hall effect due to the local quantum-interference effect-induced reduction of charge carriers. The quasi-two dimensionality of our granular arrays is confirmed by transmission electron microscopy studies and low-temperature transport behaviors. Granular CoSi₂ films are stable under ambient conditions. Their large Hall effect may benefit useful and sensitive applications.

ACKNOWLEDGMENTS

This work was supported by the National Science and Technology Council of Taiwan through Grants No. 110-2112-M-A49-015 and No. 111-2119-M-007-005 (J.-J.L.), and 110-2112-M-A49-033-MY3 (S.-S.Y.). S.-S.Y. was partly supported by the Center for Emergent Functional Matter Science of NYCU from The Featured Areas Research Center Program within the framework of the Higher Education Sprout Project by the Ministry of Education of Taiwan. The authors acknowledge the use of HRTEM at the Instrument Center of National Tsing Hua University (Taiwan).

-
- [1] B. Abeles, Ping Sheng, M. D. Coutts, and Y. Arie, Structural and electrical properties of granular metal films, *Adv. Phys.* **24**, 407 (1975).
 - [2] I. S. Beloborodov, A. V. Lopatin, V. M. Vinokur, and K. B. Efetov, Granular electronic systems, *Rev. Mod. Phys.* **79**, 469 (2007).
 - [3] Y.-J. Zhang, Z.-Q. Li, and J.-J. Lin, Logarithmic temperature dependence of Hall transport in granular metals, *Phys. Rev. B* **84**, 052202 (2011).
 - [4] J. van Lith, A. Lassesson, S. A. Brown, M. Schulze, J. G. Partridge, and A. Ayyesh, A hydrogen sensor based on tunneling between palladium clusters, *Appl. Phys. Lett.* **91**, 181910 (2007).
 - [5] K.-H. Müller, E. Chow, L. Wiczorek, B. Raguse, J. S. Cooper, and L. J. Hubble, Dynamic response of gold nanoparticle chemiresistors to organic analytes in aqueous solution, *Phys. Chem. Chem. Phys.* **13**, 18208 (2011).
 - [6] J. Herrmann, K.-H. Müller, T. Reda, G. R. Baxter, B. Raguse, G. J. B. de Groot, R. Chai, M. Roberts, and L. Wiczorek, Nanoparticle films as sensitive strain gauges, *Appl. Phys. Lett.* **91**, 183105 (2007).
 - [7] M. Huth, Granular metals: From electronic correlations to strain-sensing applications, *J. Appl. Phys.* **107**, 113709 (2010).
 - [8] M. M. A. Yajadda, I. Levchenko, and K. Ostrikov, Gold nanoresistors with near-constant resistivity in the cryogenic-to-room temperature range, *J. Appl. Phys.* **110**, 023303 (2011).
 - [9] B. I. Shklovskii, Critical behavior of the Hall coefficient near the percolation threshold, *Sov. Phys. JETP* **45**, 152 (1977).
 - [10] D. J. Bergman, Y. Kantor, D. Stroud, and I. Webman, Critical behavior of the low-field Hall conductivity at a percolation threshold, *Phys. Rev. Lett.* **50**, 1512 (1983).
 - [11] J. P. Straley, Exponent theory of the Hall effect and conductivity anisotropy near the percolation threshold, *J. Phys. C* **13**, L773 (1980).
 - [12] H. J. Juretschke, R. Landauer, and J. A. Swanson, Hall effect and conductivity in porous media, *J. Appl. Phys.* **27**, 838 (1956).
 - [13] B. Bandyopadhyay, P. Lindenfeld, W. L. McLean, and H. K. Sin, Hall effect in granular aluminum, *Phys. Rev. B* **26**, 3476 (1982).
 - [14] A. Palevski, M. Rappaport, A. Kapitulnik, A. Fried, and G. Deutscher, Hall coefficient and conduction in a 2D percolation system, *J. Physique Lett.* **45**, 367 (1984).
 - [15] X. X. Zhang, C. Wan, H. Liu, Z. Q. Li, P. Sheng, and J. J. Lin, Giant Hall effect in nonmagnetic granular metal films, *Phys. Rev. Lett.* **86**, 5562 (2001).
 - [16] S.-P. Chiu, C.-J. Wang, Y.-C. Lin, S.-T. Tu, S. K. Sahu, R.-T. Wang, C.-Y. Wu, S.-S. Yeh, S. Kirchner, and J.-J. Lin, Electronic and superconducting properties of CoSi₂ films on silicon - An unconventional superconductor with technological potential, *Chin. J. Phys.* **90**, 348 (2024).
 - [17] S.-P. Chiu, S.-S. Yeh, C.-J. Chiou, Y.-C. Chou, J.-J. Lin, and C.-C. Tsuei, Ultralow 1/f noise in a heterostructure of

- superconducting epitaxial cobalt disilicide thin film on silicon, *ACS Nano* **11**, 516 (2017).
- [18] A. H. van Ommen, C. W. T. Bulle-Lieuwma, and C. Langereis, Properties of CoSi₂ formed on (001) Si, *J. Appl. Phys.* **64**, 2706 (1988).
- [19] C.-J. Chiou, S.-P. Chiu, J.-J. Lin, and Y.-C. Chou, Effects of atomic scale imperfection at the interfaces of CoSi₂ and Si (100) on Schottky barrier contacts, *CrystEngComm* **17**, 4276 (2015).
- [20] C. Wan and P. Sheng, Quantum interference and the giant Hall effect in percolating systems, *Phys. Rev. B* **66**, 075309 (2002).
- [21] L. F. Mattheiss and D. R. Hamann, Electronic structure and properties of CoSi₂, *Phys. Rev. B* **37**, 10623 (1988).
- [22] G. C. F. Newcombe and G. G. Lonzarich, Electronic structure of cobalt disilicide, *Phys. Rev. B* **37**, 10619 (1988).
- [23] K. Radermacher, D. Monroe, A. E. White, K. T. Short, and R. Jevasinski, Quantum transport of buried single-crystalline CoSi₂ layers in (111)Si and (100)Si substrates, *Phys. Rev. B* **48**, 8002 (1993).
- [24] A. H. Van Ommen, C. W. T. Bulle-Lieuwma, J. J. M. Ottenheim, and A. M. L. Theunissen, Ion beam synthesis of heteroepitaxial Si/CoSi₂/Si structures, *J. Appl. Phys.* **67**, 1767 (1990).
- [25] Y.-N. Wu, Z.-Q. Li, and J.-J. Lin, Giant Hall effect in nonmagnetic Mo/SnO₂ granular films, *Phys. Rev. B* **82**, 092202 (2010).
- [26] D. J. Bergman and D. Stroud, *Physical Properties of Macroscopically Inhomogeneous Media* (Academic Press, 1992), pp. 147–269
- [27] A. B. Pakhomov, X. Yan, and Y. Xu, Observation of giant Hall effect in granular magnetic films, *J. Appl. Phys.* **79**, 6140 (1996).
- [28] B. Zhao and X. Yan, Giant Hall effect in granular Fe-SiO₂ film, *J. Appl. Phys.* **81**, 4290 (1997).
- [29] B. A. Aronzon, D. Y. Kovalev, A. N. Lagar'kov, E. Z. Meilikhov, V. V. Ryl'kov, M. A. Sedova, N. Negre, M. Goiran, and J. Leotin, Anomalous Hall effect in granular Fe/SiO₂ films in the tunneling-conduction regime, *JETP Lett.* **70**, 90 (1999).
- [30] J. C. Denardin, A. B. Pakhomov, M. Knobel, H. Liu, and X. X. Zhang, Ordinary and extraordinary giant Hall effects in Co-SiO₂ granular films, *J. Magn. Magn. Mater.* **226-230**, 680 (2001).
- [31] L. M. Socolovsky, C. L. P. Oliveira, J. C. Denardin, M. Knobel, and I. L. Torriani, Nanostructure of granular Co-SiO₂ thin films modified by thermal treatment and its relationship with the giant Hall effect, *Phys. Rev. B* **72**, 184423 (2005).
- [32] J. J. Lin and J. P. Bird, Recent experimental studies of electron dephasing in metal and semiconductor mesoscopic structures, *J. Phys.: Condens. Matter* **14**, R501 (2002).
- [33] B. Altshuler and A. Aronov, in *Electron-Electron Interactions in Disordered Systems*, edited by A. Efros and M. Pollak (Elsevier, Amsterdam, 1985).
- [34] Y.-C. Sun, S.-S. Yeh, and J.-J. Lin, Conductivity and tunneling density of states in granular Cr films, *Phys. Rev. B* **82**, 054203 (2010).
- [35] We use $\epsilon_r \approx 2.5$ in this estimation, which is the average of the dielectric constants of vacuum and SiO₂.
- [36] If we rewrite Eq. (2) into the more familiar AA expression $\Delta\sigma_{\square}(T) = (e^2/2\pi^2\hbar)(1 - 3\tilde{F}/4)\ln(T/T_0)$ and fit the data at $T < T_1$ to this equation, we obtain $\tilde{F} \approx -0.20$ (-0.24) for film A11 (A14).
- [37] K. B. Efetov and A. Tschersich, Coulomb effects in granular materials at not very low temperatures, *Phys. Rev. B* **67**, 174205 (2003).
- [38] I. S. Beloborodov, K. B. Efetov, A. V. Lopatin, and V. M. Vinokur, Transport properties of granular metals at low temperatures, *Phys. Rev. Lett.* **91**, 246801 (2003).